

Absence of Altermagnetic Spin Splitting Character in Rutile Oxide RuO₂

Jiayu Liu,^{1,2,3,*} Jie Zhan,^{4,5,*} Tongrui Li,^{6,*} Jishan Liu,^{2,7,†} Shufan Cheng,⁸ Yuming Shi,^{1,3} Liwei Deng,^{1,3} Meng Zhang,⁹ Chihao Li,¹⁰ Jianyang Ding,^{1,3} Qi Jiang,¹¹ Mao Ye,^{2,7} Zhengtai Liu,^{2,7} Zhicheng Jiang,⁶ Siyu Wang,⁶ Qian Li,⁶ Yanwu Xie,⁹ Yilin Wang,^{12,13} Shan Qiao,^{7,‡} Jinsheng Wen,^{8,14,§} Yan Sun,^{4,5,¶} and Dawei Shen^{6,**}

¹Shanghai Institute of Microsystem and Information Technology,
Chinese Academy of Sciences, Shanghai 200050, China

²Shanghai Synchrotron Radiation Facility, Shanghai Advanced Research Institute,
Chinese Academy of Sciences, Shanghai 201210, China

³University of Chinese Academy of Sciences, Beijing 100049, China

⁴School of Materials Science and Engineering, University of Science and Technology of China, Shenyang 110016, China

⁵Shenyang National Laboratory for Materials Science, Institute of Metal Research,
Chinese Academy of Sciences, Shenyang 110016, China

⁶National Synchrotron Radiation Laboratory and School of Nuclear Science and Technology,
University of Science and Technology of China, Hefei 230026, China

⁷National Key Laboratory of Materials for Integrated Circuits,
Shanghai Institute of Microsystem and Information Technology,
Chinese Academy of Sciences, Shanghai 200050, China

⁸National Laboratory of Solid State Microstructures and Department of Physics, Nanjing University, Nanjing 210093, China

⁹School of Physics, Zhejiang University, Hangzhou 310027, China

¹⁰Laboratory of Advanced Materials, State Key Laboratory of Surface Physics,
and Department of Physics, Fudan University, Shanghai 200438, China

¹¹Center for Transformative Science, ShanghaiTech University, Shanghai 201210, China

¹²School of Emerging Technology, University of Science and Technology of China, Hefei 230026, China

¹³Hefei National Laboratory, University of Science and Technology of China, Hefei 230088, China

¹⁴Collaborative Innovation Center of Advanced Microstructures, Nanjing University, Nanjing 210093, China

Rutile RuO₂ has been posited as a potential *d*-wave altermagnetism candidate, with a predicted significant spin splitting up to 1.4 eV. Despite accumulating theoretical predictions and transport measurements, direct spectroscopic observation of spin splitting has remained elusive. Here, we employ spin- and angle-resolved photoemission spectroscopy to investigate the band structures and spin polarization of thin-film and single-crystal RuO₂. Contrary to expectations of altermagnetism, our analysis indicates that RuO₂'s electronic structure aligns with those predicted under nonmagnetic conditions, exhibiting no evidence of the hypothesized spin splitting. Additionally, we observe significant in-plane spin polarization of the low-lying bulk bands, which is antisymmetric about the high-symmetry plane and contrary to the *d*-wave spin texture due to time-reversal symmetry breaking in altermagnetism. These findings definitively challenge the altermagnetic order previously proposed for rutile RuO₂, prompting a reevaluation of its magnetic properties.

Recently, altermagnetism (AM) has been proposed as a third fundamental magnetic phase beyond traditional ferromagnetism (FM) and antiferromagnetism (AFM) in crystals with collinear magnetic order [1–3]. In this magnetic phase, sublattices with opposite spins are connected by real-space rotation rather than translation or inversion transformation. This results in an unconventional AFM-like magnetic order with zero net magnetization, while exhibiting FM-like lifted Kramers spin degeneracy in reciprocal space [Fig. 1(a)]. This dichotomy allows altermagnets to combine the benefits of both ferromagnets and antiferromagnets, which were previously thought to be incompatible, offering advantages unparalleled by either conventional magnetic class. The unique proper-

ties of altermagnets could lead to the development of advanced materials with tailored magnetic and electronic properties, potentially revolutionizing magnetic storage and quantum computing [1, 4, 5].

Many theoretical and experimental studies have been conducted to predict and verify altermagnetic candidates in practical compounds [1, 6]. Among them, rutile oxide RuO₂ is of particular interest and has been considered one of the workhorse materials of this emerging research [7–10]. This interest is mainly rooted in predictions that rutile RuO₂ would exhibit the largest altermagnetic spin splitting, up to 1.4 eV, which could significantly enhance its potential for various spintronic applications by providing a stronger and clearer signal. Early resonant x-ray scattering [11] and neutron diffraction studies [12] identified the AFM magnetic order in RuO₂. Subsequent transport measurements on RuO₂ revealed unconventional anomalous Hall and spin-polarized currents, which could be well rationalized within the altermagnetic framework [13–17]. However, the latest independent muon-spin relaxation and rotation (μ SR) stud-

* Equal contributions

† Equal contributions; liujs@sari.ac.cn

‡ qiaoshan@mail.sim.ac.cn

§ jwen@nju.edu.cn

¶ sunyan@imr.ac.cn

** dwshen@ustc.edu.cn

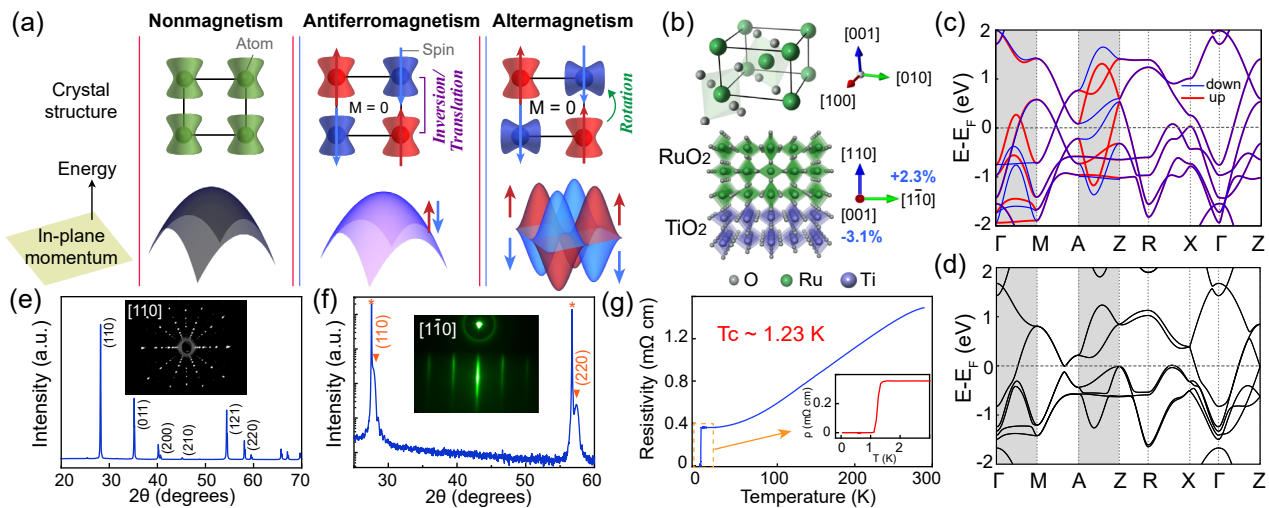


FIG. 1. The crystal structure, band structure, and characterizations of RuO_2 . (a) The categorization of the magnetism of RuO_2 : nonmagnetism, antiferromagnetism, and altermagnetism. The crystal structures in real space and corresponding band structures in reciprocal space. (b) Crystal structure of RuO_2 , lower panel: Schematic diagram of the growth of thin films RuO_2 on TiO_2 (110) substrates. (c) Energy dispersion along the high-symmetry directions for the altermagnetic phase with a static $U = 1.3$ eV correction on the Ru sites. (d) Energy dispersion for nonmagnetism of RuO_2 with the consideration of spin-orbital coupling (SOC). (e) Powder XRD of single crystal RuO_2 . Inset displays the Laue pattern along the [110] direction. (f) θ - 2θ scan of RuO_2 thin film grown on the (110)-oriented TiO_2 substrate. Bragg peaks from the TiO_2 substrates are marked with asterisks. The inset displays the RHEED pattern of the thin film. (g) Resistivity versus temperature curve of thin films.

ies, which are extremely sensitive probes to local magnetic moments, indicated an extremely small magnetically ordered moment of at most $1.4 \times 10^{-4} \mu_B/\text{Ru}$ for RuO_2 single crystals and $7.4 \times 10^{-4} \mu_B/\text{Ru}$ for thin films, respectively [18, 19]. These significantly challenged previously assumed altermagnetic ground state in rutile RuO_2 [7, 20].

Electronic structure probing techniques like angle-resolved photoemission spectroscopy (ARPES) and spin-resolved ARPES (SARPES) are capable of detecting momentum-dependent band splitting and spin polarization induced by AM [21–24]. These techniques are thus considered the gold standard for identifying AM order in compounds. Recently, ARPES and SARPES measurements have been employed to verify AM ground states in several candidates, including MnTe , MnTe_2 , and CrSb [25–30]. Given the prominence and conceptual significance of RuO_2 as a prototypical altermagnet, it is crucial to experimentally verify its altermagnetic nature from the perspective of electronic structure.

In this work, we performed ARPES and SARPES to examine the electronic structures of both thin-film and single-crystal rutile RuO_2 . We show that the Fermi surface features and band structures along the high symmetry directions are well traced by density functional theory (DFT) calculations without magnetism. The band splitting expected from altermagnetism is not observed as well. Besides, we reveal significant in-plane spin polarization of the low-lying bulk bands, which is antisymmetric about the high-symmetry plane and clearly inconsistent with the expectation of altermagnetism. Our direct spectral evidence clearly shows that RuO_2 is highly unlikely to be an altermagnet.

Figure 1(b) presents the crystal structure of rutile RuO_2 with the space group $P4_2/mnm$, where ruthenium(Ru) atoms are located at the centers of oxygen octahedra [31]. Neighboring oxygen octahedra are connected through rotation rather than translation, which would result in a typical d -wave altermagnetic ground state if the spins at Ru sites were aligned antiferromagnetically. Our first-principles calculations reveal spin splitting along the Γ – M and A – Z directions [Fig. 1(c)], consistent with previous predictions of the AM state [32, 33]. These bands are distinct from the nonmagnetic case shown in Fig. 1(d), where all bands are degenerate. Thus, directly investigating the low-lying band structure and corresponding spin polarization should be an effective method for identifying the magnetic ground state of rutile RuO_2 . Given that previous μSR studies have thoroughly explored the magnetically ordered moments of both RuO_2 single crystals and thin films, we conducted ARPES and SARPES measurements on both types of samples to achieve comprehensive results. For detailed descriptions of sample syntheses, (S)ARPES measurements and first-principles calculations, please refer to the methods section in the Supplementary Material, note 1 [34]. Note that the substrate-induced strain on the thin films does not alter the magnetic ground states according to our calculations (see details in Supplementary Material, note 2). Figure 1(e) shows the powder x-ray diffraction (XRD) and Laue patterns of RuO_2 single crystals. Figure 1(f) presents the high resolution XRD and RHEED patterns of the epitaxial thin films. These demonstrate the high quality and atomically flat surface of the samples. Moreover, the superconducting transition temperature reaches up to 1.23 K [Fig. 1(g)],

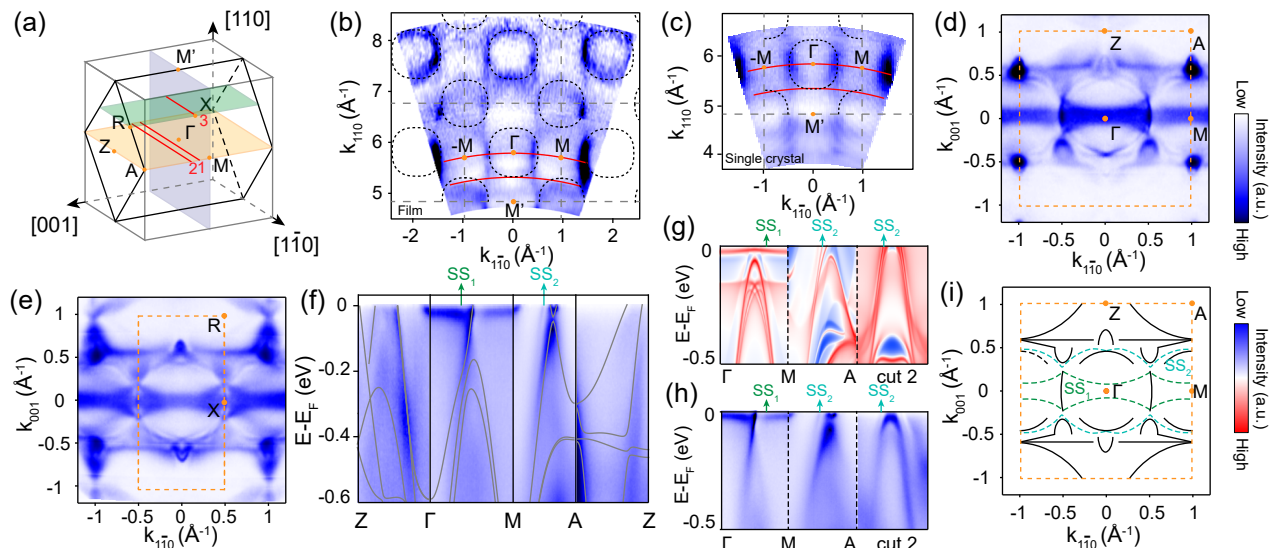


FIG. 2. Fermi surfaces and dispersions of RuO₂. (a) 3D BZ of RuO₂, with yellow and green planes showing high symmetry planes Γ - M - A - Z and R - X . (b),(c) Photon emission intensity maps of thin films and single crystals along the out-of-plane direction, compiled over photon energy ranges from 82–300 eV and 50–160 eV, respectively. Gray dotted squares represent the BZ, and black dashed lines mark the Fermi surface for nonmagnetic calculations. (d),(e) Fermi surface maps of the high symmetry planes Γ - M - A - Z and R - X , measured at photon energies of 124 and 103 eV, respectively. (f) Energy dispersions along high symmetry directions. Gray solid lines represent nonmagnetic calculated bulk bands. SS₁ and SS₂ are surface states. (g),(h) Calculated surface band dispersions and the corresponding photoemission plots, respectively. (i) Schematic of the Fermi surface, including bulk and surface states.

comparable to the highest recorded among all reported values [35–37], further demonstrating the superior quality of our thin films for *in-situ* ARPES and SARPES measurements.

A prerequisite for identifying possible altermagnetic spin splitting in the low-energy electronic structure of RuO₂ is the elimination of interference from complex surface states [32]. To achieve this, we conducted detailed photon-energy-dependent ARPES measurements to distinguish surface and bulk states near the Fermi level (E_F). Figures 2(b) and 2(c) present photoemission intensity maps in the k_{110} - $k_{1\bar{1}0}$ plane [the gray plane in the three-dimensional Brillouin zone (BZ) in Fig. 2(a)] taken at E_F for thin films and single crystals, respectively. Both maps clearly show periodic alternation of large and slightly smaller circular Fermi pockets, which can be well reproduced by our nonmagnetic bulk band calculations (black dashed rings). Additionally, both maps exhibit nearly dispersionless chainlike features along the tangents of these pockets, which were not captured by our calculations, indicating their surface band nature.

We investigated detailed the low-lying band structure on both high-symmetry planes Γ - M - A - Z and R - X [light yellow and light green planes shown in Fig. 2(a), respectively] to directly compare them to calculations. The corresponding photoemission intensity maps and plots taken from the single-crystal RuO₂ are shown in Figs. 2(d)–2(f). Despite the complexity of the intertwined surface and bulk band structures, we could unambiguously recognize surface states (labeled as SS₁ and SS₂) by comparing theoretically determined surface band dispersions

[Fig. 2(g)] with the corresponding photoemission plots [Fig. 2(h)]. It is crucial to pinpoint all surface states as the extra surface bands can easily be misinterpreted as AM-induced spin splitting. We reached the similar conclusion using thin film data (Supplemental Material, note 3) and schematically summarized our findings in Fig. 2(i), which are consistent with previous reports [38–40]. We found that the bulk band dispersions along high-symmetry directions shown in Fig. 2(f) are in remarkable agreement with the nonmagnetic calculations (light gray lines), implying that RuO₂ is more likely a paramagnetic metal.

We next examined the alignment of experimental bulk bands with magnetic and nonmagnetic calculations along high-symmetry directions Γ - M [Fig. 3(a)], Γ - Z [Fig. 3(e)], and three other typical cuts across the BZ [Figs. 3(b)–3(d), cuts 1–3 illustrated in Fig. 2(a)]. According to the proposed AM state in RuO₂, all these low-lying bulk bands should exhibit lifted spin degeneracy except for those along Γ - Z , which are connected by the screw rotation operation $S_{4z} = \{C_{4z}|(1/2, 1/2, 1/2)\}$. However, along Γ - M , we could only identify three bulk bands near the E_F : the electronlike α band crossing E_F , and two holelike β and γ bands with band tops located at ~ 0.2 eV and 0.4 eV below E_F , respectively. Using momentum distribution curves (MDCs) and second derivative plot [Fig. 3(a) ii], we precisely extracted dispersions of three bands and appended them onto the photoemission intensity plot [black dashed line in Fig. 3(a) i]. No band splitting predicted by the magnetic calculations was found in our data. We note the energy resolution of our

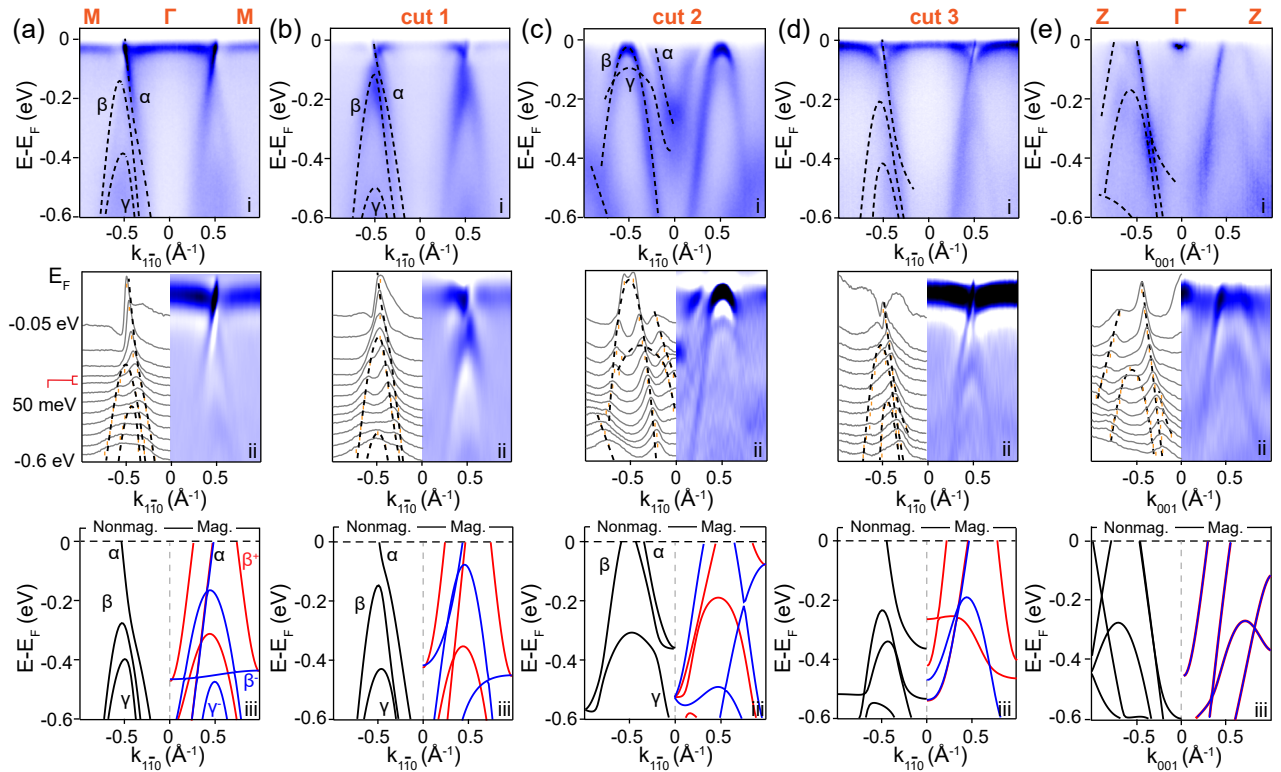


FIG. 3. Comparisons of calculated energy dispersions in nonmagnetic and alternative magnetic states. (a)-(e) The photoemission plots at different momentum (i), momentum distribution curves, and the second derivative plots (ii), comparisons of nonmagnetic and magnetic calculations (iii). Red and blue lines represent spin-up and spin-down states, respectively. Cut 3 was acquired at a photon energy of 103 eV, and the other four cuts at 124 eV.

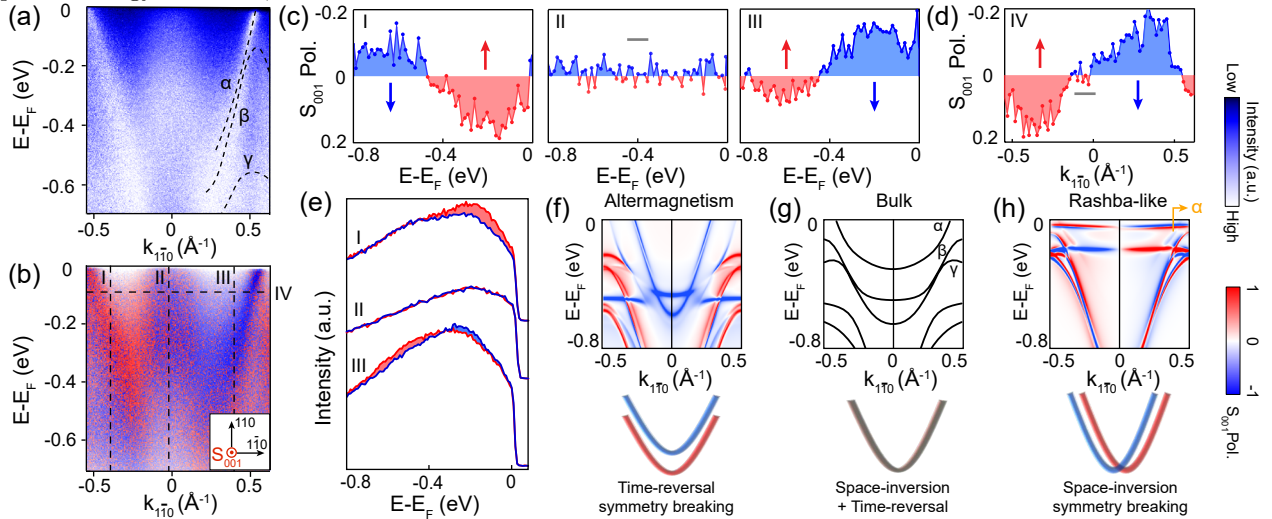


FIG. 4. Spin polarization in RuO₂. (a) Spin-integrated band dispersion. (b) Spin polarization of the bulk band dispersion. (c) Spin polarization versus binding energy at different momenta indicated by the black dashed line in (b). (d) Spin polarization versus momentum at the binding energy of around 0.1 eV. (e) Spin-resolved energy distributed curves at the three selected momenta. (f)–(h) Surface spin projected band structure of alternative magnetic state (f), bulk band structure of nonmagnetic state (g), surface spin projected band structure of nonmagnetic state (h) and corresponding schematic diagrams of system's symmetry.

experiments and emphasize that no spin splitting higher than 10 meV was observed (Fig. S4 of Supplemental Material). Figures 3(b) and 3(c) illustrate the evolution of three bulk bands with momentum. We observed that the α and β bands move upwards in binding energy from the

cut along Γ – M to cut 2, while the top of the γ band initially falls and then rises. This complex evolution of all three bulk bands can be qualitatively captured by nonmagnetic calculations, and no signs of the spin splitting suggested by the AM state calculations. Figure 3(d) is

the photoemission intensity plot along cut 3, showing all three bulk bands similar to those along Γ — M , which is in good agreement with nonmagnetic calculations rather than AM predictions [Fig. 3(d) iii]. Figure 3(e) presents a comparison of our ARPES results along Γ — Z with DFT calculations. Because of screw rotation symmetry protection, even the AM state prediction does not show lifted Kramer spin degeneracy [Fig. 3(e) iii]. Note that the band in the nonmagnetic calculations has been shifted to match the band dispersion [Fig. S5 of Supplemental Material]. We observed only one band crossing E_F within the momentum range of 0 to 0.5 \AA^{-1} , which conflicts with the AM prediction of two bands crossing E_F . We performed a similar comparison on thin film, as detailed in Fig. S6 of Supplemental Material. Overall, our ARPES data, whether taken from single crystals or thin films, are more consistent with nonmagnetic calculations.

In addition to using band splitting as a criterion, incorporating spin-polarized band characterization could provide more compelling evidence for determining the presence of an AM state [1, 28]. Therefore, we conducted SARPES experiments using a helium lamp with photon energy of 21.2 eV [41]. Figure 4(a) illustrates the spin-integrated ARPES result of thin-film RuO₂ taken along a cut parallel to Γ — M while located close to the X — R plane. The electronlike band could be identified as the bulk α band [Fig. 4(g)] and referring to Fig. 3(d). The S_{001} -resolved photoemission intensity plot is shown in Fig. 4(b), in which this bulk band exhibit pronounced opposite spin polarizations for electrons of opposite momentum. Figures 4(c) and 4(e) display the S_{001} polarization versus binding energy and spin-resolved energy distribution curves (EDCs) taken at three different momenta, respectively. Additionally, the S_{001} polarization as a function of momentum at around 0.1 eV below E_F is presented in Fig. 4(d). All these data suggest that the bulk band is highly spin polarized, with an in-plane polarization vector S_{001} antisymmetric about the Γ — Z — M' high-symmetry plane. This finding sharply contrasts with the mainstream prediction of the AM state, where the α band should be fully spin polarized but symmetric about the high-symmetry plane, as suggested in Fig. 4(f) and Fig. S7. We emphasize that our SARPES findings are robust, as similar results were obtained from multiple thin-film and single-crystal samples (Supplemental Material, note 8).

The spin polarization structure observed in RuO₂ is really intriguing for both space-inversion and time-reversal symmetries are preserved, and thus there should be no spin splitting, as schematically shown in Fig. 4(g). We speculate that the Rashba-like spin splitting may be due to the breaking of the space-inversion symmetry as the penetration depth of photoelectrons excited is only around 10 Å in real experiments. Figure 4(h) presents the calculated spin polarization of low-lying bands contributed mainly from states in the top several layers

of RuO₂, simulated through the Green's function calculations. Figure S9 also shows slab calculations that yield Rashba-like states. This simulation exhibits evident space-inversion symmetry breaking and is qualitatively consistent with our SARPES findings. Furthermore, the presence of oxygen vacancies would break both the inversion symmetry of the space group and the central symmetry of the Ru site point group, which would inherently gift the bulk band structure with spin polarization attributes (Fig. S10 in Supplemental Material, note 1). In short, the observed Rashba-like splitting ambitiously ruling out the possibility of magnetism.

In summary, we utilize ARPES and SARPES to directly examine the band structures and spin polarization of thin-film and single-crystal rutile RuO₂ samples. Our results show that electronic structure of RuO₂ matches well with nonmagnetic conditions. We did not observe the momentum-dependent spin splitting that was expected from the AM state. Furthermore, we detect significant in-plane spin polarization in the low-lying bulk bands, which is antisymmetric relative to the high-symmetry plane and incompatible with the d -wave spin texture expected from time-reversal symmetry breaking in AM. Our work would stimulate further experimental and theoretical research in AM, underscoring the need for reconsidering both material candidates and theoretical models, while the observed unusual spin polarization may have a great potential application in spintronics. In addition, the anomalous spin polarization in RuO₂ may be closely related to the catalytic performance as RuO₂ has been proven to be a useful potential catalyst for energy conversion and storage applications.

Acknowledgements

This work is supported by the National Key R&D Program of China (No. 2023YFA1406304), National Science Foundation of China (No. U2032208, No. 12004405, No. 52271016, No. 52188101), Anhui Provincial Natural Science Foundation (No. 2408085J003). J.S.W. is supported by National Key Projects for Research and Development of China (No. 2021YFA1400400) and National Natural Science Foundation of China (No. 12225407 and No. 12074174). Y.L.W. is supported by the Innovation Program for Quantum Science and Technology (No. 2021ZD0302800) and the National Natural Science Foundation of China (No. 12174365). Y.W.X. is supported by the National Natural Science Foundation of China (No. 12325402). S.Q. is supported by the National Natural Science Foundation of China (Grants No. 11927807 and No. U2032207). Z.C.J. acknowledges the China National Postdoctoral Program for Innovative Talents (BX20240348). Part of this research used Beamline 03U of the Shanghai Synchrotron Radiation Facility, which is supported by ME² project under Contract No. 11227902 from National Natural Science Foundation of China. Part of the numerical calculations in this study were carried out on the ORISE Supercomputer (No. DFZX202319).

-
- [1] L. Šmejkal, J. Sinova, and T. Jungwirth, Beyond conventional ferromagnetism and antiferromagnetism: A phase with nonrelativistic spin and crystal rotation symmetry, *Phys. Rev. X* **12**, 031042 (2022).
- [2] Z. Savitsky, Researchers discover new kind of magnetism, *Science* **383**, 574 (2024).
- [3] L. Šmejkal, J. Sinova, and T. Jungwirth, Emerging research landscape of altermagnetism, *Phys. Rev. X* **12**, 040501 (2022).
- [4] S. Bhowal, and N. A. Spaldin, Ferroically ordered magnetic octupoles in d-wave altermagnets, *Phys. Rev. X* **14**, 011019 (2024).
- [5] P. Khalili Amiri, C. Phatak, and C. Finocchio, Prospects for antiferromagnetic spintronic devices, *Annu. Rev. Mater. Res.* **54** (2024).
- [6] L. Bai *et al.*, Altermagnetism: Exploring new frontiers in magnetism and spintronics, arxiv:2406.02123.
- [7] A. Smolyanyuk, I. I. Mazin, L. Garcia-Gassull, and R. Valentí, Fragility of the magnetic order in the prototypical altermagnet RuO₂, *Phys. Rev. B* **109**, 134424 (2024).
- [8] R. M. Sattigeri, G. Cuono, and C. Autieri, Altermagnetic surface states: towards the observation and utilization of altermagnetism in thin films, interfaces and topological materials, *Nanoscale* **15**, 16998 (2023).
- [9] A. Ptok, Ruthenium dioxide RuO₂: Effect of the altermagnetism on the physical properties, arxiv:2309.02421.
- [10] L. Šmejkal, A. B. Hellenes, R. González-Hernández, J. Sinova, and T. Jungwirth, Giant and tunneling magnetoresistance in unconventional collinear antiferromagnets with nonrelativistic spin-momentum coupling, *Phys. Rev. X* **12**, 011028 (2022).
- [11] Z. Zhu *et al.*, Anomalous antiferromagnetism in metallic RuO₂ determined by resonant x-ray scattering, *Phys. Rev. Lett.* **122**, 017202 (2019).
- [12] T. Berlijn *et al.*, Itinerant antiferromagnetism in RuO₂, *Phys. Rev. Lett.* **118**, 077201 (2017).
- [13] Z. Feng *et al.*, An anomalous hall effect in altermagnetic ruthenium dioxide, *Nat. Electron.* **5**, 735 (2022).
- [14] L. Šmejkal, R. González-Hernández, T. Jungwirth, and J. Sinova, Crystal time-reversal symmetry breaking and spontaneous Hall effect in collinear antiferromagnets, *Sci. Adv.* **6**, eaaz8809 (2020).
- [15] R. González-Hernández *et al.*, Efficient electrical spin splitter based on nonrelativistic collinear antiferromagnetism, *Phys. Rev. Lett.* **126**, 127701 (2021).
- [16] H. Bai *et al.*, Efficient spin-to-charge conversion via altermagnetic spin splitting effect in antiferromagnet RuO₂, *Phys. Rev. Lett.* **130**, 216701 (2023).
- [17] S. Karube *et al.*, Observation of spin-splitter torque in collinear antiferromagnetic RuO₂, *Phys. Rev. Lett.* **129**, 137201 (2022).
- [18] M. Hiraishi *et al.*, Nonmagnetic ground state in RuO₂ revealed by muon spin rotation, *Phys. Rev. Lett.* **132**, 166702 (2024).
- [19] P. Keßler *et al.*, Absence of magnetic order in RuO₂: Insights from μ SR spectroscopy and neutron diffraction, arxiv:2405.10820.
- [20] M. Wenzel *et al.*, Fermi-liquid behavior of non-altermagnetic RuO₂, arXiv:2407.11148.
- [21] H. Zhang *et al.*, Angle-resolved photoemission spectroscopy, *Nat. Rev. Methods Primers* **2**, 54 (2022).
- [22] B. Lv, T. Qian, and H. Ding, Angle-resolved photoemission spectroscopy and its application to topological materials, *Nat. Rev. Phys.* **1**, 609 (2019).
- [23] G. Schönhense, K. Medjanik, and H.-J. Elmers, Space-, time- and spin-resolved photoemission, *J. Electron. Spectrosc. Relat. Phenom.* **200**, 94 (2015).
- [24] T. Okuda, Recent trends in spin-resolved photoelectron spectroscopy, *J. Phys. Condens. Matter* **29**, 483001 (2017).
- [25] J. Ding *et al.*, Large band-splitting in *g*-wave type altermagnet CrSb, arxiv:2405.12687.
- [26] G. Yang *et al.*, Three-dimensional mapping and electronic origin of large altermagnetic splitting near Fermi level in CrSb, arxiv:2405.12575.
- [27] S. Reimers *et al.*, Direct observation of altermagnetic band splitting in CrSb thin films, *Nat. Commun.* **15**, 2116 (2024).
- [28] J. Krempaský *et al.*, Altermagnetic lifting of Kramers spin degeneracy, *Nature (London)* **626**, 517 (2024).
- [29] Y.-P. Zhu *et al.*, Observation of plaid-like spin splitting in a noncoplanar antiferromagnet, *Nature (London)* **626**, 523 (2024).
- [30] S. Lee *et al.*, Broken kramers degeneracy in altermagnetic MnTe, *Phys. Rev. Lett.* **132**, 036702 (2024).
- [31] C. A. Occhialini *et al.*, Local electronic structure of rutile RuO₂, *Phys. Rev. Res.* **3**, 033214 (2021).
- [32] Z. Lin *et al.*, Observation of giant spin splitting and d-wave spin texture in room temperature altermagnet RuO₂, arxiv:2402.04995.
- [33] K.-H. Ahn, A. Hariki, K.-W. Lee, and J. Kuneš, Antiferromagnetism in RuO₂ as *d*-wave Pomeranchuk instability, *Phys. Rev. B* **99**, 184432 (2019).
- [34] See Supplemental Material at <URL> for additional data of the ARPES experiment and other results, which includes Refs. [7, 36–39, 41–54].
- [35] C. A. Occhialini *et al.*, Strain-modulated anisotropic electronic structure in superconducting RuO₂ films, *Phys. Rev. Mater.* **6**, 084802 (2022).
- [36] J. P. Ruf *et al.*, Strain-stabilized superconductivity, *Nat. Commun.* **12**, 59 (2021).
- [37] M. Uchida, T. Nomoto, M. Musashi, R. Arita, and M. Kawasaki, Superconductivity in uniquely strained RuO₂ films, *Phys. Rev. Lett.* **125**, 147001 (2020).
- [38] V. Jovic *et al.*, Dirac nodal lines and flat-band surface state in the functional oxide RuO₂, *Phys. Rev. B* **98**, 241101 (2018).
- [39] V. Jovic *et al.*, Momentum for catalysis: How surface reactions shape the RuO₂ flat surface state, *ACS Catal.* **11**, 1749 (2021).
- [40] V. Jovic *et al.*, The Dirac nodal line network in non-symmorphic rutile semimetal RuO₂, arXiv:1908.02621.
- [41] H. Zha *et al.*, Improvement of image-type very-low-energy-electron-diffraction spin polarimeter, *Rev. Sci. Instrum.* **94** (2023).
- [42] X. Lu *et al.*, Dimensionality-controlled evolution of charge-transfer energy in digital nickelates superlattices, *Adv. Sci.* **9**, 2105864 (2022).
- [43] J. Ding *et al.*, Strain-induced modulation of electronic structure in correlated Dirac semimetal P_v-CaIrO₃ epitaxial thin films, *J. Vac. Sci. Technol., A* **42** (2024).
- [44] Y.-C. Yang *et al.*, High-resolution ARPES endstation for

- in situ electronic structure investigations at SSRF, Nucl. Sci. Tech. **32**, 31 (2021).
- [45] G. Kresse, and J. Furthmüller, Efficient iterative schemes for *ab initio* total-energy calculations using a plane-wave basis set, Phys. Rev. B **54**, 11169 (1996).
- [46] S. L. Dudarev, G. A. Botton, S. Y. Savrasov, C. Humphreys, and A. P. Sutton, Electron-energy-loss spectra and the structural stability of nickel oxide: An LSDA + U study, Phys. Rev. B **57**, 1505 (1998).
- [47] O. Fedchenko *et al.*, Observation of time-reversal symmetry breaking in the band structure of altermagnetic RuO₂, Sci. Adv. **10**, eadj4883 (2024).
- [48] A. A. Mostofi *et al.*, wannier90: A tool for obtaining maximally-localised Wannier functions, Comput. Phys. Commun. **178**, 685 (2008).
- [49] Q. Wu, S. Zhang, H.-F. Song, M. Troyer, and A. A. Soluyanov, Wanniertools: An open-source software package for novel topological materials, Comput. Phys. Commun. **224**, 405 (2018).
- [50] M. L. Sancho, J. L. Sancho, J. L. Sancho, and J. Rubio, Highly convergent schemes for the calculation of bulk and surface Green functions, J. Phys. F **15**, 851 (1985).
- [51] A. Manchon, H. C. Koo, J. Nitta, S. M. Frolov, and R. A. Duine, New perspectives for Rashba spin-orbit coupling, Nat. Mater. **14**, 871 (2015).
- [52] Y. Feng *et al.*, Rashba-like spin splitting along three momentum directions in trigonal layered PtBi₂, Nat. Commun. **10**, 4765 (2019).
- [53] X. Zhang, Q. Liu, J.-W. Luo, A. J. Freeman, and A. Zunger, Hidden spin polarization in inversion-symmetric bulk crystals, Nat. Phys. **10**, 387 (2014).
- [54] K. Gotlieb *et al.*, Revealing hidden spin-momentum locking in a high-temperature cuprate superconductor, Science **362**, 1271 (2018).